First results of humidity sensors based on CeO2 thick film deposited by a new deposition technique from a suspension of nanoparticles

T. Toloshniak, Y. Guhel, A. Besq, B. Boudart

First results of humidity sensors based on CeO_2 thick film deposited by a new deposition technique from a suspension of nanoparticles

T. Toloshniak[1], Y. Guhel[2*], A. Besq[3], and B. Boudart[2]

[1]Prodways Impression 3D, ZI Les Garennes, 78130 Les Mureaux - France

[2]Normandie Univ, UNICAEN, ENSICAEN, CNRS, GREYC, 14000 Caen - France

[3]Normandie Univ, UNICAEN, ABTE, 14000 Caen - France

* Author who is to check the proofs
Yannick.guhel@unicaen.fr
Telephone: (33) 2 33 01 40 06 Fax: (33) 2 31 45 26 98

Keywords: cerium oxide, humidity sensor, thick films, oxygen vacancies.

Abstract

In this paper, we show the possibility to deposit a CeO_2 thick film on (111) silicon substrate from a suspension of CeO_2 nanoparticles by a new process of thick layer deposition in order to realize a humidity sensor. This new technique is derived from the spin-coating technology. The suspension is based on ultra-fine grinding of CeO_2 firstly in a stirred media mill coupled then in a sonication cell. Suspension viscosity has been adjusted with carbopol polymer and its rheological properties have been analyzed in order to cover completely the silicon substrate by the CeO_2 layer. Then, the impact of a conventional annealing on the crystallinity of the CeO_2 film has also been investigated by Raman spectroscopy and by scanning electron microscopy. Finally, gold interdigitated electrodes have been screen printed on the thick film surface in order to realize a sensor and first promising results on the humidity sensitivity have been highlighted.

1. Introduction

In the last decade, humidity sensors have gained increasing interest because monitoring and controlling humidity is not only useful in many industrial processes such as in automotive, agriculture, alimentary, pharmaceutical, and semiconductors industries but also in domestic electrical appliances [1-3]. Humidity sensors suitable in these practical applications require a high and linear response, a fast response, a recovery behavior, a small hysteresis, a wide humidity detection range, a long-term stability, and a low cost [4]. The performances of humidity sensors are mainly related to the properties of the sensing materials. So, a wide variety of materials for humidity sensors have been studied such as ceramic [1, 3, 5], organic polymer [6, 7], metal oxides [8-11], porous silicon [12], nano-porous silicon arrays [13], carbon nanotubes [14], cerium oxide nanowires, cerium oxide nanoparticles [4, 15-18] and multi-walled carbon nanotube thin films [19]. Many papers have reported on studies concerning the humidity sensitivity of metal oxide using Al_2O_3 [20-22], TiO_2 [10, 23-25], SnO_2 [9, 26, 27], TiO_2-SnO_2 [8], ZnO [9, 11, 28] and ZrO_2 [29, 30] as sensing material. In fact, metal oxide materials have been mainly investigated due to their chemical and physical stability, high mechanical strength and wide operating temperature range [17, 31]. Several recent papers have highlighted the interest of nanostructured metal oxide material for the realization of humidity sensors because of their high surface to volume ratio and eventual changes in physical and chemical properties resulting from the quantum size effect [31]. Moreover, nanometer materials are characterized by small grain size and large specific surface area leading to more surface-active sites and a better sensitivity [29]. For these reasons, a focus on nanometer materials as Al_2O_3 nanotubes [22], nanocrystalline TiO_2 films [10], TiO_2 nanotubes [25], SnO_2 particles [26], SnO_2 nanowires [27], ZnO nanowires [32], ZnO

materials [11], ZnO nanorods [28], ZrO_2 nanorods [30], CeO_2 nanowires [15, 16], and CeO_2 nanoparticles [17, 18] has been done. For the latter material, Thakur et al. [4, 17] have recently reported that the sensors exhibit a high and linear response within the entire relative humidity (RH) ranging from 11 up to 97% at an operating frequency of 60 Hz. At the same time, the impedance of the sensor changes from $3.91x10^8$ down to $3.58x10^5$ Ω when RH increases from 11 up to 97%. Then the response and recovery times are approximately 3 and 16 s, respectively. A high sensitivity and a good linearity have also been highlighted by Xie et al. for sensor based on CeO_2 nanoparticles [18]. Effectively, they have shown that the complex impedance modulus decreases from $3.8x10^7$ down to $4.3x10^3$ Ω when the relative humidity rises from 11 up to 98% and that the response and recovery times were 10 and 3 s, respectively. Fast humidity sensors based on CeO_2 nanowires have also been done [15, 16] and response and recovery times of 3 s have been obtained. In the literature, CeO_2 materials can be made using different well known growth methods notably in the field of microelectronics, as pulsed laser deposition, sputtering, organic chemical vapor deposition, molecular beam epitaxy [33-42]….

However, it also possible to use other techniques such as spray pyrolysis [43], sol-gel process [44], hydrothermal method [15], rapid microwave-assisted method [17], solvothermal method [18], and sonochemical [45] methods. Once again, it is important to point out that low cost technologies must be involved to realize humidity sensors [4, 16, 17]. Accordingly, spin coating of CeO_2 suspension could be a new way to realize humidity sensors, which must be assessed.

In this paper, we present a new methodology developed in order to deposit by spin coating a CeO_2 thick layer on silicon substrate and the characterization of the film as well as its humidity sensitivity.

We have used an aqueous suspension of grinded CeO_2 particles with a rheological behavior adjusted with carbopol polymer (Ultrez 21 grade, Noveon). This polymer is a hydrophobically modified crosslinked polyacrylate polymer designed to efficiently impart thickening, stabilizing, and suspending properties to a variety of personal care applications. This product self-wets quickly and easily without any mixing required. It also exhibits improved electrolyte tolerance that is interesting for complex formulation. Depending on carbopol concentration and pH solution, the mechanical behaviors range from purely viscous solutions to elastoplastic gels. An extended review of the mechanical characteristics of the carbopol gels has been done by Piau [46].

The aim of this paper is to investigate in a first time the preparation of CeO_2 particles suspensions and their rheological properties, and silicon substrate treatment as well, in order to cover it. In a second time, the goal is to characterize the CeO_2 thick films formed and to study the modification induced by a conventional annealing. Non-annealed and annealed thick layers have been characterized by scanning electron microscopy (SEM) and by Raman spectroscopy. Finally, gold interdigitated electrodes have been deposited on the annealed thick films to realize a capacitive sensor, which has been tested in humidity to determine its sensitivity. The reported results are very promising and highlight that the capacitance increases with relative humidity. To our best knowledge, it is the first time that humidity sensors are fabricated with such technique.

2. Experimental

All experiments conducted in this study have been carried out with cerium oxide (99.9% purity) powder manufactured by Alfa Aesar. As powder granulometry is closed to 10 µm, a grinding stage was required for the deposition of thick films on silicon substrate by spin-coating. Effectively, some little uncovered zones can exist on the substrate if the grain size is too large and it is difficult to completely cover the silicon substrate in these conditions. For these reasons, it was imperative to grind it in order to uniformly cover the silicon substrate and to deposit a film thickness inferior to 10 µm. Firstly, the suspension was prepared by using 50 g of CeO_2 powder, 70 ml of deionized water and 2 ml of Dolapix CA (organic deflocculating agent) in order to form a slurry which is then poured in a bottle containing 470 g of yttria stabilized zirconia balls (1.2 mm diameter). A grinding and mixing stage either 24 or 48 h was operated with a rotary overhead shaker (Reax 20, Heidolph) at 10 rpm. Balls have been then removed and mixing was continuously done to prevent any agglomeration via sedimentation of this raw suspension. Rotation was stopped only for pipetting samples for further batch preparations dedicated to spin-coating deposition. The volume of a batch was fixed to 20 ml and consists in a mix of raw CeO_2 suspension, deionized water and 24 h hydrated carbopol solution (Ultrez 21 grade, Noveon) at 1% w/w. Because of basic pH of the CeO_2 suspension, direct swollen of carbopol particles occurs leading to an increase of viscosity and a limited sedimentation. Pipetting volumes (HandyStep electronic, Brand) of each element were adjusted in order to obtain a suspension with different carbopol concentrations ranging from 0 to 0.3% w/w and a fixed CeO_2 concentration (0.24 g/ml).

As sonication is a common way to break up agglomerates and promote dispersion of particles into base fluids, the batch mixture was dispersed and grounded using an

ultrasonic horn Bandelin Sonopuls HD3200 with a titanium tapered tip KE76. Operating power was set to 40% with a 0.5 s pulse and 0.5 s relaxation cycles applied during 40 s. This maximum admissible amplitude was limited because of the high-density energy dissipation (fluid temperature elevation) and the life duration of the tip considerations (erosion phenomena).

Flow measurements have been carried out at 20 °C with a control stress rheometer (AR1000N, TA Instruments) and a cone-plate geometry (40 mm diameter and 1° angle) in order to determine rheological properties of preparations. The plate of the rheometer was the same silicon substrate used for spin-coating depositions. The silicon wafer (2'') was simply sticked onto the rheometer.

The particle size distribution (PSD) of the grain dispersed in the CeO_2 suspension was characterized by using a Horiba LA-950 laser granulometer.

Type (111) silicon substrates with an 2-20 Ω.cm resistivity was chosen for all experiments. Surface treatment retained was realized either with acetone or a diluted hydrofluoric acid (HF) during 5 minutes, whether for the purpose of spin-coating or for rheometry.

In the first stage of spin-coating process, the mix carbopol-CeO_2 was deposited as a droplet (500 µl) onto the substrate. In the second stage, the substrate was accelerated (5000 rpm/s) to a prescribed rotational speed (3000 rpm) during 30 s. The coating procedure was repeated six times in order to increase the CeO_2 film thickness and to fully cover the substrate. Then CeO_2 layer was first dried on a hotplate at 200 °C during 1 h in order to improve the adhesion of the CeO_2 film on the silicon substrate and to evaporate the water. Then, it was annealed at 1350 °C during 6 h under air atmosphere in a tubular furnace in order to densify the thick film and also to eliminate the carbon compounds.

The thickness of the annealed CeO_2 layer is 6.5 µm and has been measured by using a profilometer.

The morphology of the CeO_2 films was studied by scanning electron microscopy by using Hitachi S3460N and Tescan-Mira equipments and their crystallinity was characterized by using both UV and visible Raman spectroscopy in order to analyze the surface and the bulk.

An InVia Renishaw Raman spectrometer was used in a backscattering configuration at room temperature. The excitation sources used were helium-cadmium and helium-neon lasers with a wavelength of 325 (UV) and 633 nm (visible), respectively. UV and visible Raman spectra of the different samples were performed with 40 X or 50 X objectives, respectively. The position (δ) and the full width at half maximum (Γ) of the Raman lines were extracted by fitting with Lorentzian and Gaussian model. The measurement dispersion was depending on the slight inhomogeneities of the CeO_2 layers and the accuracy of the spectrometer. It has been estimated from statistical analysis at 0.2 and 0.3 cm^{-1} for δ and Γ, respectively.

The humidity sensors were made by depositing gold interdigitated electrodes on the top of the CeO_2 thick layer by screen printing technique. The sensors were placed in a Secasi hot/cold oven with a moisture rate regulated from 5 up to 95% at a temperature of 25 °C. The capacitance values of the sensors were measured with an LCR Fluke PM 6306 meter.

3. Results and discussion

Typically, particles in suspension used for spinning process are colloidal (20-300 nm) and film thickness is in the order of several hundreds of nanometers [47]. As the raw CeO_2 powder used in this study presents a monomodal distribution of the particle

size centered at 10 µm (Fig. 1), it was imperative to grind it in order to uniformly cover the silicon substrate. The mixing and ball grinding of the CeO_2 suspension followed by sonication stage lead to a significant particle size reduction as depicted by PSD in Fig. 1.

After a rotary milling of 24 h (Fig. 1-a), the main mode of the PSD is slightly shifted and the PSD becomes broader because of apparition of smaller size particles (lower limit 0.2 µm) and the existence of non-grounded particles. This observation corresponds to a soft mechanical stripping and debulking of particles, especially considering SEM micrograph of raw particles (Fig. 2-a). The effects of the sonication stage are much more important. The PSD becomes trimodal with a mode corresponding to the original population, which is much less significant and shifted toward 20 µm. The main new mode is centered on 670 nm and is associated to disrupting of mechanically crushed particles and those stressed by the grinding. Smaller particles (80 nm mean size) are also observed but they are a minority. Contrary to the previous milling step, a 48 h period is sufficient to fractionize all the particles of the raw CeO_2 powder (Fig. 1-b). A bimodal PSD is obtained with two modes observed previously and centered at 580 and 80 nm respectively, with the first one, which predominates. Sonication leads once again to a new particle size reduction. Weak size evolution is observed and particle numbers adjustment is mainly concerned. The 580 nm population decreases (with a slight shift to 510 nm) to the benefit of the one centered at 80 nm. The minimum size, which can be obtained with these operations, seems to be 40 nm and the maximum size still remains important and is 8 µm. It is worth noting that this latter methodology ensures good-reproducibility as highlighted by the PSD obtained with two different batches (Fig. 1-b). For these reasons, the subsequent preparation for spin-coating experiments have been obtained by following this protocol. At least, both smaller modes, 510/670 nm and 80 nm,

are achieved with 24 and 48 h ball milling period but 80 nm species are found only for a grinding period of 48 h. This observation is also shown by SEM micrographs (Figs. 2-b and 2-c). The SEM image of CeO_2 raw powder indicates the 500-600 nm population exists initially in an agglomerated form (Fig. 2-a).

The desired characteristics of spin-coated films include uniformity in thickness and morphology and absence of pinholes and other mechanical defects. Fluid rheology has been reported as an important property impacting film profile [48, 49]. For colloidal suspension, inter-particles forces and local solid fraction drive the shear thinning behavior [49]. Large viscosity changes could thus occur for small changes in concentration due to film spreading as indicated by Regh et al. for non-hard sphere colloidal suspension [47]. For these reasons, the behavior of CeO_2 suspension must be studied by rheological measurements and we have analyzed them in the context of rheological behaviors of two commercial photoresists that are LOR (Microchem) and S1805 (Shipley). These products are known to easily cover a silicon substrate by using spin coating technique and they are commonly used in photolithography process for microelectronic applications. The flow curves (i.e. shear stress versus shear rate data) of photoresists and CeO_2 grinded/sonicated suspension are reported in Fig. 3. The 0.24 g/ml CeO_2 suspension is a low viscous Newtonian fluid (2.3 mPa.s). This viscosity is lower than the viscosity of Newtonian S1805 photoresist (6.7 mPa.s). A more viscous with a low shear thinning behavior is observed for LOR photoresist. We consider the constitutive equation corresponding to the power law model [50]:

$$\tau = K\,\dot{\gamma}^{n}$$

where τ (Pa), K (Pa.s), $\dot{\gamma}$ (s^{-1}) and n (dimensionless) are shear stress, consistency index, shear rate and power law index.

Fitting the data, the values of K and n are equal to 0.223 and 0.95, respectively. The power law index is close to 1. This agrees with the low shear-thinning behavior of LOR photoresist. It is interesting to note that the power law index would be equal to 1 if the fluid behavior was Newtonian.

Insofar as rheometric tests concern low viscous fluids and are performed on a rotational rheometer (control torque device), experimental precautions are required. Shear rate range should be adjusted in order to respect the low-torque limit. The air bearing of the instrument allows virtually friction free application of torque but any real air bearing presents internal friction torque, which must be considered for low viscous fluids. The small variations can be mapped as a function of the angular position. This rotational mapping has been realized with software option set to 3 iterations. Fluid surface tension should not produce a torque in rotational rheometers based on the idealized assumption of rotational symmetry. Recently, it has been demonstrated that this principle could be infringed because finite deviation of the contact line symmetry and fluid/geometry interface angle symmetry can produce a significant torque in case of low viscous fluids [51]. Sample loading and proper sample volume must be carefully set to control as much as possible the contact line. For our experiments, best practices leading to a pure Newtonian response have been found by using low viscous standard silicon oil and micropipette. All the data reported in Fig. 3 correspond to a silicon substrate systematically degreased with acetone before each test.

Another important phenomenon to pay special attention concerns the sedimentation because it will directly influence the uniformity of spinning films and affect rheometric tests. As settling time of CeO_2 particles is short enough, rheometric tests consist in a fast decreasing shear rate sweep starting with fluid highly sheared during

2 min. As the impact of inertia contribution becomes then significant for low viscous fluids, the inertia instrument correction has been applied.

Considering rheological behavior of raw CeO_2 suspension and sedimentation, it is imperative to increase the viscosity of the CeO_2 suspension up to the range of photoresists and to stabilize particles while limiting the shear-thinning behavior.

For this purpose, Carbopol Ultrez 21 was selected and three mass concentrations have been studied to prepare fluids dedicated to spin coating process. Rheometric tests were carried out immediately following fluid preparation (Fig. 3).

We can see that all systems present a shear-thinning behavior and moreover, the increase of the viscosity depends directly on carbopol mass. Both 0.15 and 0.2% carbopol concentration show an evolution in logarithmic scale suggesting that there is no surface tension effect and this true shear-thinning behavior could be fit with the power law model. We can also note that their rheological behaviors become similar for the high shear rate indicating that the system behaves as non-interacting CeO_2 particles flowing in a media with a constant viscosity. The 0.3% carbopol concentration highlights a viscosity level more important and the non-Newtonian behavior is more pronounced. Moreover, the low shear rate deviation (below 1 s^{-1}) indicates surface tension torque effect.

Nevertheless, it is important to note that the silicon substrate is perfectly covered when the LOR and S1805 photoresists are deposited by spin-coating while they have a shear thinning and Newtonian behaviors, respectively. For these reasons, the carbopol concentration of 0.3% has been excluded for spin coating experiments and the 0.2% carbopol concentration has been retained because the silicon substrate seems better covered in comparison with 0.15 carbopol concentration.

Furthermore, as the silicon substrate needs a hydrofluoric acid treatment before

the deposition in order to etch the native oxide layer, which can exist, this hydrophobic surface has been used to study the rheological effects even if this confined flow can't give further indication of quality deposition by spin-coating. However, the rheological behavior of the CeO_2 suspension with a carbopol concentration of 0.2% after a HF treatment has been compared with that after an acetone treatment because the previous studies were done after an acetone treatment, as in Fig. 3 for example.

Thus, we can see that the rheological curves concerning the CeO_2 suspension with a 0.2% carbopol concentration after an acetone treatment or after a HF treatment are located between the LOR photoresist and S1805 photoresist curves, as shown in Fig. 4. Moreover, flow curves for fluid with 0.2% carbopol concentration realized with a new grinded/sonicated batch show that same shear thinning behavior is observed for shear rate higher than 1 s^{-1}. No surface tension effect is still observed for the silicon substrate degreased whereas low shear rate plateau appears for the HF treatment. This suggests that interface angle is affected. It could be also wall slip through changes in fluid-surface interactions. Indeed, hydrophobic surfaces allow noticeable slip because of small dipole moment of polar liquids [52] and nanobubbles at solid-liquid interface [53].

Thus, fluid-surface interactions seem to be determinant for deposition scenario. Regh et al. interestingly remark that local charge distribution on the substrate may influence film structure and film thinning for suspension [47]. A theoretical approach of particle transport and aggregation assuming a Newtonian behavior in a spin-coating process highlights that adhesive properties of the particles and substrate influence the deposition process [54].

In summary, it is difficult to affirm that the HF treatment is clearly better than acetone treatment for the CeO_2 suspension deposition by spin-coating. However, we think

that the quality of the Si/CeO_2 interface should be better if the native oxide layer was etched before the deposition. We have observed that the adhesion of CeO_2 nanoparticles on the silicon substrate is better after a HF acid treatment than after an acetone treatment. The reproducibility of the technological process using the HF acid treatment is also better than that using the acetone treatment. Thus, we have decided to clean the silicon surface with the HF treatment before the deposition of thick layers.

Thick CeO_2 layers have been deposited by spin-coating with the 0.2% carbopol suspension and HF treated silicon substrate. Then, after a drying stage at 200 °C, the CeO_2 layers have been annealed at 1350 °C for 6 h under air atmosphere. The morphology and the crystallinity have been characterized by scanning electron microscopy and Raman spectroscopy. SEM micrographs of CeO_2 thick layers before and after an annealing performed at 1350 °C during 6 h under air atmosphere are shown in Fig. 5. An increase in CeO_2 grain size has been observed after annealing. Moreover, the presence of pores has also been highlighted with the non-annealed (Fig. 5-a) and annealed CeO_2 layer (Fig. 5-b) but the pores seem more visible after annealing.

Then the CeO_2 thick films were analyzed by visible Raman spectroscopy in order to analyze the layer crystallinity. In fact, the position, the line width, the line shape, and the intensity of the Raman peaks are depending on the vibrational state of the studied material and therefore δ and Γ of the Raman band are impacted by the stress state, the crystalline quality and the measurement temperature. Effectively, a fine Γ has stood for a good material crystalline quality.

Fig. 6 presents the visible Raman spectra of a CeO_2 thick film deposited on a (111) Si substrate by spin-coating before and after a post-annealing performed at 1350 °C for 6 h under air atmosphere.

Before annealing, two separate Raman bands are highlighted at 465.5 and 521.4 cm^{-1} that are the signatures of the triply degenerate Raman active mode of the CeO_2 thin film [55] and to the longitudinal optical mode of the Si substrate [56], respectively. In this visible Raman spectrum, the F_{2g} Raman band is attributed to the cubic fluorite phase [57, 58]. After the annealing, the Raman line related to CeO_2 thick film increases from 465.5 up to 466.2 cm^{-1} and the Γ of Raman peak related to CeO_2 layer decreases from 9.5 down to 8.3 cm^{-1}. Then these values are compared with those obtained with a CeO_2 powder considered like a stress-free material and taken as a reference (δ = 465 cm^{-1}, Γ = 8.2 cm^{-1}) [59] in order to analyze the impact of post-annealing on the CeO_2 layer crystallinity. Thus, we note that Γ is close to the reference that confirms a good crystalline quality of the post-annealed CeO_2 films. However, the Raman position is clearly superior to the reference value. This is explained by a compressive strain in relation to the Si substrate [60]. Moreover, the CeO_2 layers have been characterized by UV Raman spectroscopy because the low penetration depth (close to 30 nm) of the UV radiation into the material allows to obtain a Raman signal coming from the CeO_2 layer and not from the silicon substrate [57]. For these reasons, non-annealed and annealed CeO_2 films have also been characterized by UV Raman spectroscopy with a laser wavelength of 325 nm. Moreover, the gap value of the band gap energy for a CeO_2 film [61, 62] is analogous to the excitation energy and therefore it is possible to observe the resonance Raman effects. In these conditions, the multi-phonon scattering is activated and multi-order Raman modes are present in the Raman spectra [60].

Fig. 7 shows that UV Raman spectra of CeO_2 thick films before and after annealing are different. In fact, we can observe five Raman lines located at values close to 464.3, 586.5, 1172.4, 1555.2, and 1755.6 cm^{-1} for the annealed CeO_2 layer but no

Raman line centered at 586.5 cm^{-1} was observed on the Raman spectrum of non-annealed CeO_2 film. So, the Raman line located at 464.3 cm^{-1} is ascribed to the triply degenerate Raman active mode (F_{2g}) of the CeO_2 thin film [55] and those found at 1172.4 and 1755.6 cm^{-1} can correspond to a second-order longitudinal optical mode (2LO) and to a third-order longitudinal optical mode (3LO), respectively [55, 58, 59, 63]. The small Raman line located at 1555.2 cm^{-1}, meanwhile, is attributed to a band related to physisorbed O_2 [64]. However, the identification of the Raman line located at 586.5 cm^{-1} is more difficult because this broad band is attributed to a disorder band, which is generally named D [58, 59, 65]. Moreover, we have already studied the origin of D band by UV Raman spectroscopy in a previous paper [66], and we have highlighted that the D band was originated from the combination of two bands which are attributed to the presence of oxygen vacancies and of Ce^{3+} ions in CeO_2 thin layer, respectively. So, we can affirm that the Raman band centered at 586.5 cm^{-1} is attributed to the presence of oxygen vacancies and Ce^{3+} ions in CeO_2 thick layer deposited on silicon substrate by spin coating. Effectively, the emergence of oxygen vacancies in a CeO_2 layer can be correlated with the reduction of Ce^{4+} to Ce^{3+} [65, 67].

As for the characterization done by visible Raman spectroscopy, we can note that the annealing has also induced a decrease in the F_{2g} Raman peak linewidth from 48.3 down to 11.4 cm^{-1}, which is induced by an improvement of the CeO_2 layer crystallinity. These results are confirmed by the presence of the multi-phonon Raman structures of the third order in the UV Raman spectrum before and after the annealing, that confirms a good crystallinity of the CeO_2 thick layer in the two cases [68]. For these reasons, we cannot consider that the reduction in Γ is only induced by an improvement of the

crystallinity of the CeO_2 thick layer because Γ also depends on the crystallite size [55]. In fact, the evolution of Γ versus the crystallite size (D) is given by the following relation:

$$\Gamma = a + \frac{b}{D}$$

where a and b are constants depending of the material and the unit of Γ and D are cm^{-1} and nm, respectively.

In these conditions, we can say that the reduction in Γ is explained by the improvement of the crystallinity of the CeO_2 layer and/or by an increase in the crystallite size as shown in Fig. 5. Moreover, the annealing has involved the apparition of oxygen vacancies and Ce^{3+} ions in the film. We think that the annealing involves the reaction between the silicon substrate and the CeO_2 layer that implies the creation of oxygen vacancies and the Ce^{4+} to Ce^{3+} cations transformation. Indeed, it is known that oxidized silicon and/or an amorphous silicide layer appears after an annealing done at high temperature. These interfacial reactions occur simultaneously with a reduction of Ce^{4+} to Ce^{3+} [69, 70].

It is important to specify that the measurements by Raman spectroscopy have been done in many areas on the thick layers and all the results obtained from Raman spectra are reproducible and highlight that the CeO_2 layer is homogeneous.

In order to evaluate the humidity sensing characteristics of the CeO_2 thick film, gold interdigitated electrodes have been deposited on the top of the CeO_2 thick layer (as shown in the inset in Fig. 8) by screen printing technique. The capacitance (C) measurements have been done at a frequency of 200 Hz at a temperature of 20 °C.

Fig. 8 presents the evolution of the sensor capacitance versus the relative humidity. In fact, the capacitance varies slightly from 0.9 up to 1.2 nF when RH rises from 5 up to 25%. Then C increases sharply from 1.2 up to 63 nF when RH changes from

25 up to 93%. Moreover, the value of C is nearly recovered when RH drops from 93 down to 5%, as shown in Fig. 8. It is important to note that the capacitance is intimately linked to the dielectric coefficient of the sensing material and consequently to its polarization properties. So, a rise of the relative humidity induces an increase in the adsorbed water molecules onto the sensing material surface, and consequently the polarization is stronger and the dielectric coefficient and capacitance are higher [71]. Besides a low change in the capacitance is observed in the low RH range in Fig. 8 because few water molecules are adsorbed onto the surface of sensing CeO_2 material, that involves a weak polarization and accordingly a low capacitance. For higher RH, the adsorbed water molecules concentration is more important and therefore the polarization is stronger and the capacitance higher [72]. Moreover, the capacitance depends on both dielectric constants of CeO_2 layer and of water. Effectively this phenomenon can also explain the increase in capacitance with the relative humidity. In fact, the dielectric constant of the water (80 [72]) is clearly higher than that of CeO_2 layers (26 [73]). So, we can think that the pores existing in the CeO_2 film fill with water molecules as the RH increases which induces an increase in capacitance [72]. We can add that the high relative humidity water vapor starts to condense in the pores of the CeO_2 layers by capillary effect, even when the partial pressure in the vapor is below saturation. Therefore, we can assume that the water vapor condensation in the pores induces an increase in capacitance as it has been already observed with porous silicon layer [12] and amorphous Al_2O_3 nanotubes [72].

The presence of oxygen vacancies in the CeO_2 thick layer can also be a factor impacting the humidity sensitivity as highlighted for ZrO_2 nanorods [30]. In these conditions, the oxygen vacancies can act as highly active sites for water adsorption. This phenomenon is consistent with our CeO_2 layer characterization by UV Raman

spectroscopy because we have highlighted the presence of oxygen vacancies in the annealed thick films. In summary, the humidity sensitivity is explained by an increase in the dielectric constant of CeO_2 thick layer and by the presence of oxygen vacancies in the CeO_2 thick layer.

4. Conclusion

In this paper, we have presented a new technique in order to deposit a CeO_2 thick film on a (111) silicon substrate. To our knowledge, it is the first time that such technique is reported. Firstly, a suspension done from CeO_2 powder, Dolapix and deionized water is grinded by a rotary milling for 48 h and then by a sonication for 40 s in order to decrease the CeO_2 particle size. Secondly, 0.2% of carbopol polymer has been added to adjust the viscosity of the suspension. The carbopol polymer concentration has been chosen on the basis of rheometric characterization results. Thirdly, the CeO_2 suspension adjusted with the carbopol polymer has been deposited by spin-coating and annealed at 1350 °C for 6 h under air atmosphere. A good crystallinity of annealed film has been highlighted by Raman spectroscopy but the presence of oxygen vacancies has been observed. A humidity sensor has been done on the CeO_2 thick film and we have shown that the capacitance increases from 0.9 up to 63 nF when the relative humidity changes from 5 up to 93%. These first results are very promising because this humidity sensor has been performed by using a new and low-cost technique. Of course, this original method needs to be optimized in order to improve the performances of the sensor but the aim of this paper is to present a new technique to realize a low-cost humidity detector. This technique can also be used in order to realize other types of sensors using other materials.

Acknowledgments

The authors would like to thank J. Bernard and J. El Fallah for their technical assistance.

REFERENCES

[1] E. Traversa, “Ceramic sensors for humidity detection: the state-of-the-art and future developments”, Sens. Actuators B 23 (1995) 135-156.

[2] Z. Chen, C. Lu, “Humidity Sensors: A Review of Materials and Mechanisms”, Sensor. Lett. 3 (2005) 274-295.

[3] J. Shah, R.K. Kotnala, B. Singh, H. Kishan, “Microstructure-dependent humidity sensitivity of porous $MgFe_2O_4$-CeO_2 ceramic”, Sens. Actuators B 128 (2007) 306-311.

[4] V.R. Khadse, S. Thakur, K.R. Patil, P. Patil, “Humidity-sensing studies of cerium oxide nanoparticles synthesized by non-isothermal precipitation”, Sens. Actuators B 203 (2014) 229-238.

[5] N. Yamazoe, Y. Shimizu, “Humidity sensors: Principles and Applications”, Sens. Actuators 10 (1986) 379-398.

[6] G. Delapierre, H. Grange, B. Chambaz, L. Destannes, “Polymer-based capacitive humidity sensor: Characteristics and Experimental Results”, Sens. Actuators 4 (1983) 97-104.

[7] Y. Sakai, Y. Sadaoka, M. Matsuguchi, “Humidity Sensors based on polymer thin films”, Sens. Actuators B 35-36 (1996) 85-90.

[8] W-P. Tai, J-H. Oh, “Fabrication and humidity sensing properties of nanostructured TiO_2-SnO_2 thin films”, Sens. Actuators B 85 (2002) 154-157.

[9] S.P. Yawale, S.S. Yawale, G.T. Lamdhade, “Tin oxide and zinc based doped humidity sensors”, Sens. Actuators A 135 (2007) 388-393.

[10] K.P. Biju, M.K. Jain, “Effect of crystallization on humidity sensing properties of sol-gel derived nanocrystalline TiO_2 thin films”, Thin Solid Films 516 (2008) 2175-2180.

[11] B.C. Yadav, R. Srivastava, C.D. Dwivedi, P. Pramanik, “Moisture sensor based on ZnO nanomaterial synthesized through oxalate route”, Sens. Actuators B 131 (2008) 216-222.

[12] S-J. Kim, J-Y. Park, S-H. Lee, S-H. Yi, “Humidity sensors using porous silicone layer with mesa structure”, J. Phys. D: Appl. Phys. 33 (2000) 1781-1784.

[13] Y.Y. Xu, X.J. Li, J.T. He, X. Hu, H.Y. Wang, “Capacitive humidity sensing properties of hydrothermally-etched silicone nano-porous pillar array”, Sens. Actuators B 105 (2005) 219-222.

[14] C.L. Cao, C.G. Hu, L. Fang, S.X. Wang, Y.S. Tian, C.Y. Pan, “A capacitive Humidity Sensor Based on Multi-Wall Carbon Nanotubes (MWCNTs)”, Sensors. (2009) 9 (9) 7431-7444.

[15] X.Q. Fu, C. Wang, H.C. Yu, Y.G. Wang, T.H. Wang, “Fast humidity sensors based on CeO_2 nanowires”, Nanotechnology 18 (2007) 145503-1-145503-4.

[16] Z. Zhang, C. Hu, Y. Xiong, R. Yang, Z.L. Wang, “Synthesis of Ba-doped CeO_2 nanowires and their application as humidity sensors”, Nanotechnology 18 (2007) 465504-1-465504-5.

[17] S. Thakur, P. Patil, “Rapid synthesis of cerium oxide nanoparticles with superior humidity-sensing performance”, Sens. Actuators B 194 (2014) 260-268.

[18] W. Xie, B. Liu, S. Xiao, H. Li, Y. Wang, D. Cai, D. Wang, L. Wang, Y. Liu, Q. Li, T. Wang, “High performance humidity sensors based on CeO_2 nanoparticles”, Sens. Actuators B 215 (2015) 125-132.

[19] C.L. Cao, C.G. Hu, L. Fang, S.X. Wang, Y.S. Tian, and C.Y. Pan, “Humidity Sensor Based on Multi-Walled Carbon Nanotube Thin Films”, J. Nanomater. Article ID 707303, (2011) 1-5.

[20] R.K. Nahar, V.K. Khanna, “Ionic doping and inversion of the characteristic of thin film porous Al_2O_3 humidity sensor”, Sens. Actuators B 46 (1998) 35-41.

[21] L. Juhasz, A. Vass-Varnai, C. Dminkovics, V. Timar-Horvath, “Porous Al_2O_3 Layers for Capacitive RH Sensor”, Second international symposium Advanced Micro- and Mesoporous Materials (2007) Bulgária.

[22] B. Cheng, B. Tian, C. Xie, Y. Xiao, S. Lei, “High sensitive humidity sensor based on amorphous Al_2O_3 nanotubes”, J. Mater. Chem. 21 (2011) 1907-1912.

[23] B.C. Yadav, A.K. Srivastava, P. Sharma, “Resistance Based Humidity Sensing Properties of TiO_2”, Sensors & Transducers Journal 81 (2007) 1348-1353.

[24] L.L.W. Chow, M.M.F. Yuen, P.C.H. Chan, A.T. Cheung, “Reactive sputtered TiO_2 thin film humidity sensor with negative substrate bias”, Sens. Actuators B 76 (2001) 310-315.

[25] Q. Wang, Y.Z. Pan, S.S. Huang, S.T. Ren, P. Li, J.J. Li, “Resistive and capacitive response of nitrogen-doped TiO_2 nanotubes film humidity sensor”, Nanotechnology 22 (2011) 025501-1-025501-11.

[26] M. Parthibavarman, V. Hariharan, C. Sekar, “High-sensitivity humidity sensor based on SnO_2 nanoparticles synthesized by microwave irradiation method”, Mater. Sci. Eng. C 31 (2011) 840-844.

[27] Q. Kuang, C. Lao, Z.L. Wang, Z. Xie, L. Zheng, “High-Sensitivity Humidity Sensor Based on a single SnO_2 Nanowire”, J. Am. Chem. Soc. 129 (2007) 6070-6071.

[28] Y. Zhang, K. Yu, D. Jiang, Z. Zhu, H. Geng, L. Luo, “Zinc oxide nanorod and nanowire for humidity sensor”, Appl. Surf. Sci. 242 (2005) 212-217.

[29] J. Wang, M.Y. Su, J-Q. Qi, L-Q. Chang, “Sensitivity and complex impedance of nanometer zirconia thick humidity sensors”, Sens. Actuators B 139 (2009) 418-424.

[30] Y. Lu, Z. Wang, S. Yuan, L. Shi, Y. Zhao, W. Deng, “Microwave-hydrothermal synthesis and humidity sensing behavior of ZrO_2 nanorods”, RSC Adv. 3 (2013) 11707-11714.

[31] P. Biswas, S. Kundu, P. Banerji, S. Bhunia, “Super rapid rsponse of humidity sensor based on MOCVD grown ZnO nanotips array”, Sens. Actuators B 178 (2013) 331-338.

[32] S-P. Chang, S-J. Chang, C-Y. Lu, M-J. Li, C-L. Hsu, Y-Z. Chiou, T-J. Hsueh, I-C. Chen, “A ZnO nanowire-based humidity sensor”, Superlattices and Microstruct. 47 (2010) 772-778.

[33] J. Kang, X. Liu, G. Lian, Z. Zhang, G. Xiong, X. Guan, R. Han, Y. Wang, “Crystal-orientation controlled epitaxial CeO_2 dielectric thin films on Si(100) substrates using pulsed laser deposition”, Microelectron. Eng. 56 (2001) 191-194.

[34] B. Hirschauer, G. Chiaia, M. Göthelid, U.O. Karlsson, “Studies of highly oriented CeO_2 films grown on Si(111) by pulsed laser deposition”, Thin Solid Films 348 (1999) 3-7.

[35] S. Gnanarajan, N. Savvides, “Evolution of texture of CeO_2 thin film buffer layers prepared by ion-assisted deposition”, Thin Solid Films 350 (1999) 124-129.

[36] L. Kim, J. Kim, D. Jung, C.Y. Park, C.W. Yang, Y. Roh, “Effects of deposition parameters on the crystallinity of CeO_2 thin films deposited on Si(100) substrates by r.f.-magnetron sputtering”, Thin Solid Films 360 (2000) 154-158.

[37] M.T. Ta, D. Briand, Y. Guhel, J. Bernard, J.C. Pesant, B. Boudart, “Growth and structural characterization of cerium oxide thin films realized on Si(111) substrates by on-axis r.f. magnetron sputtering”, Thin Solid Films 517 (2008) 450-452.

[38] T. Inoue, M. Ohashi, N. Sakamoto, S. Shida, “Orientation selective epitaxial growth of CeO_2 layers on Si(100) substrates using reactive DC magnetron sputtering with substrate bias”, J. Crystal Growth 271 (2004) 176-183.

[39] M. Paranthaman, A. Goyal, F.A. List, E.D. Specht, D.F. Lee, P.M. Martin, Q. He, D.K. Christen, D.P. Norton, J.D. Budai, D.M. Kroeger, “Growth of biaxially textured buffer layers on rolled-Ni substrates by electron beam evaporation”, Physica C 275 (1997) 266-272.

[40] S. Ikegawa, Y. Motoi, “Growth of CeO_2 thin films by metal-organic molecular beam epitaxy”, Thin Solid Films 281-282 (1996) 60-63.

[41] D. Barreca, G. Bruno, A. Gasparotto, M. Losurdo, E. Tondello, “Nanostructure and optical properties of CeO_2 thin films obtained by plasma-enhanced chemical vapor deposition”, Mater. Sci. Eng. C 23 (2003) 1013-1016.

[42] Y. Kim, Y. Gao, G.S. Herman, S. Thevuthasan, W. Jiang, D.E. McCready, S.A. Chambers, “Growth and structure of epitaxial CeO_2 by oxygen-plasma-assisted molecular beam epitaxy”, J. Vac. Sci. Technol. A 17 (1999) 926-936.

[43] B. Elidrissi, M. Addou, M. Regragui, C. Monty, A. Bourgrine, A. Kachouane, “Structural and optical properties of CeO thin films prepared by spray pyrolysis”, Thin Solid Films 379 (2000) 23-27.

[44] N. Phonthammachai, M. Rumruangwong, E. Gulari, A.M. Jamieson, S. Jitkarnka, S. Wongkasemjit, “Synthesis and rheological properties of mesoporous nanocrystalline CeO_2 via sol-gel process”, Colloids and Surfaces A: Eng. Aspects 247 (2004) 61-68.

[45] D.V. Pinjari, A.B. Pandit, “Room temperature synthesis of crystalline CeO_2 nanopowder: Advantage of sonochemical method over conventional method”, Ultrasonics Sonochemistry 18 (2011) 1118-1123.

[46] J. M. Piau, “Carbopol gels: Elastoviscoplastic and slippery glasses made of individual swollen sponges: Meso-and macroscopic properties, constitutive equations and scaling laws.”, J. Non-Newtonian Fluid Mech. 144 (2007) 1-29.

[47] T. J. Rehg, G. Higgins, “Spin coating of colloidal suspensions”, AIChE J. 38 (1992) 489-501.

[48] S.A. Jenekhe, S. B. Schuldt, “Coating flow of non-Newtonian fluids on a flat rotating disk”, Ind. Eng. Chem. Fundamen. 23 (1984) 432-436.

[49] J. A. Britten, I. M. Thomas, “Non-Newtonian flow effects during spin coating large-area optical coatings with colloidal suspensions”, J. Appl. Phys. 71 (1992) 972-979.

[50] G.W. Scott Blair, J.C. Hening, A. Wagstall, “The flow of cream through narrow glass tubes”, J. Phys. Chem. 43 (1939) 853-864.

[51] M.T. Johnston, R. H. Ewoldt, “Precision rheometry: Surface tension effects on low-torque measurements in rotational rheometers”, J. Rheol. 57 (2013) 1515-1532.

[52] J.-H. J. Cho, B. M. Law, F. Rieutord, “Dipole-Dependent Slip of Newtonian Liquids at Smooth Solid Hydrophobic Surfaces”, Phys. Rev. Lett. 92 (2004) 166102-1-166102-4.

[53] E. Ruckenstein, P. Rajora, “On the no-slip boundary condition of hydrodynamics”, J. Colloid Interface Sci. 96 (1983) 488-491.

[54] Y. Zhao, J. S. Marshall, “Spin coating of a colloidal suspension”, Phys. Fluids, 20 (2008) 043302-1-043302-15.

[55] W.H. Weber, K.C. Hass, J.R. McBride, “Raman study of CeO_2: Second-order scattering, lattice dynamics, and particle-size effects”, Phys. Rev. B 48 (1993) 178-185.

[56] I. De Wolf, “Stress measurements in si microelectronics devices using Raman spectroscopy”, J. Raman Spectr. 30 (1999) 877-883.

[57] T. Taniguchi, T. Watanabe, N. Sugiyama, A.K. Subramani, H. Wagata, N. Matsushita, M. Yoshimura, “Identifying Defects in ceria-Based Nanocrystals by UV Resonance Raman spectroscopy”, J. Phys. Chem. C 113 (2009) 19789-19793.

[58] Z. Wu, M. Li, J. Howe, H.M. Meyer III, S.T. Overbury, “Probing Defect Sites on CeO_2 Nanocrystals with Well-defined Surface Planes by Raman Spectroscopy and O_2 adsorption”, Langmuir. 26 (2010) 16595-16606.

[59] Y. Guhel, M.T. Ta, J. Bernard, B. Boudart, J.C. Pesant, “Raman characterization before and after rapid thermal annealing of CeO_2 thin films grown by rf sputtering on (111) Si”, J. Raman Spectr. 40 (2009) 401-404.

[60] B. Boudart, Y. Guhel, J.C. Pesant, P. Dhamelincourt, M.A. Poisson, “Raman characterization of Mg^+ ion-implanted GaN”, J. Phys.: Condens. Matter 16 (2004) S49–S55.

[61] S. Debnath, M.R. Islam, M.S.R. Kahn, “Optical properties of CeO_2 thin films”, Bull. Mater. Sci. 30 (2007) 315-319.

[62] J.T. Jones, P.M. Bridger, O.J. Marsh, T.C. McGill, “Charge storage in CeO_2/Si/CeO_2/Si(111) structures by electrostatic force microscopy”, Appl. Phys. Lett. 75 (1999) 1326-1328.

[63] J.E. Spanier, R.D. Robinson, F. Zhang, S.W. Chan, I.P. Herman, “Size-dependent properties of CeO_{2-y} nanoparticles as studied Raman scattering”, Phys. Rev. B 64 (2001) 245407-1-245407-8.

[64] V.V. Pushkarev, V.I. Kovalchuk, J.L. d’Itri, “Probing Defect Sites on the CeO_2 Surface with Dioxygen”, J. Phys. Chem. B 108 (2004) 5341-5348.

[65] A. Sokiou, S. Ntais, V. Dracopoulos, S. Papaefthimiou, G. Leftheriotis, P. Yianoulis, “Substrate related structural, electronic and electrochemical properties of evaporated CeO_x ion storage layers”, Thin Solid Films 514 (2006) 87-96.

[66] T. Toloshniak, Y. Guhel, J. Bernard, A. Besq, S. Marinel, B. Boudart, “Impact of microwave annealing on CeO_2 thin films sputtered on (111) Si”, Mater. Res. Bull.70 (2015) 712-718.

[67] M. Swanson, V.V. Pushkarev, V.I. Kovalchuk, J.L. d’Itri, “The dynamics surface chemistry during the interaction of CO with ceria captured by Raman spectroscopy”, Catal. Lett. 116 (2007) 41-45.

[68] B. Boudart, Y. Guhel, J. C. Pesant, P. Dhamelincourt, M. A. Poisson, “Raman characterization of Ar^+ ion-implanted GaN”, J. Raman Spectr. 33 (2002) 283-286.

[69] ‘X-ray investigation of annealed CeO2 films prepared by sputtering on Si substrates’,

I. Iordanova, L. Popova, P. Aleksandrova, G. Beshkov, E. Vlahkov, R. Mirchev, B. Blagoev,

Thin Solid Films 515, pp. 87-96, 2007.

[70] ‘Grain growth and mechanical properties of CeO2-x films deposited on Si (100) substrates by pulsed dc magnetron sputtering’,

I.W. Park, J. Lin, J.J. Moore, M. Khafizov, D. Hurley, M.V. Manuel, T. Allen

Surface & Coating Technology, 217, pp. 34-38, 2013.

[71] J. Wang, H. Wui, Q. Lin, “Properties of a nanocrystalline barium titanate on silicon humidity sensor”, Meas. Sci. Technol. 14 (2003) 172-175.

[72] B. Cheng, B. Tian, C. Xie, Y. Xiao, S. Lei, “Highly sensitive humidity sensor based on amorphous Al_2O_3 nanotubes”, J. Mater. Chem. 21 (2011) 1907-1912.

[73] L. Cossarutto, N. Chaoui, E. Millon, J.F. Muller, J. Lambert, M. Alnot, "CeO_2 thin films on Si(100) obtained by pulsed laser deposition", Appl. Surf. Sci. 126 (1998) 352-355.

FIGURE CAPTIONS

Fig. 1: Influence of rotary grinding and sonication on the particle size distribution of the CeO_2 suspension for a grinding time of 24 h (Fig. 1-a) or 48 h (Fig. 1-b).

Fig. 2: SEM micrographs before grinding (2-a), after a rotary milling of 24 h and a sonication (2-b) and after a rotary milling of 48 h and a sonication (2-c).

Fig. 3: Rheological behaviors of CeO_2 suspension without carbopol and with a carbopol mass concentration of 0.15, 0.2 and 0.3%, LOR photoresist and S1805 photoresist.

Fig. 4: Rheological behaviors of S1805 and LOR photoresists, CeO_2 suspension with a viscosity adjusted with 0.2% carbopol polymers concentration on the silicon substrate treated with acetone or hydrofluoric acid.

Fig. 5: SEM micrographs of CeO_2 layers before and after an annealing performed at 1350 °C for 6 h under air atmosphere.

Fig. 6: Raman spectra of CeO_2 thick film deposited by spin coating on a (111) Si substrate before and after an annealing performed at 1350 °C for 6 h under air atmosphere. Raman spectra were obtained with a laser wavelength of 633 nm. The inset is a zoom of the spectra.

Fig. 7: Raman spectra of CeO_2 thick film deposited by spin coating on a (111) Si substrate before and after an annealing performed at 1350 °C for 6 h under air atmosphere. Raman spectra were obtained with a laser wavelength of 325 nm.

Fig. 8: Influence of the relative humidity on the capacitance of a sensor performed on a CeO_2 thick layer deposited by spin coating on a silicon substrate. The square is the

value of the capacitance obtained after the humidity exposure. The inset is a schematic representation of the sensor.

Figure 1

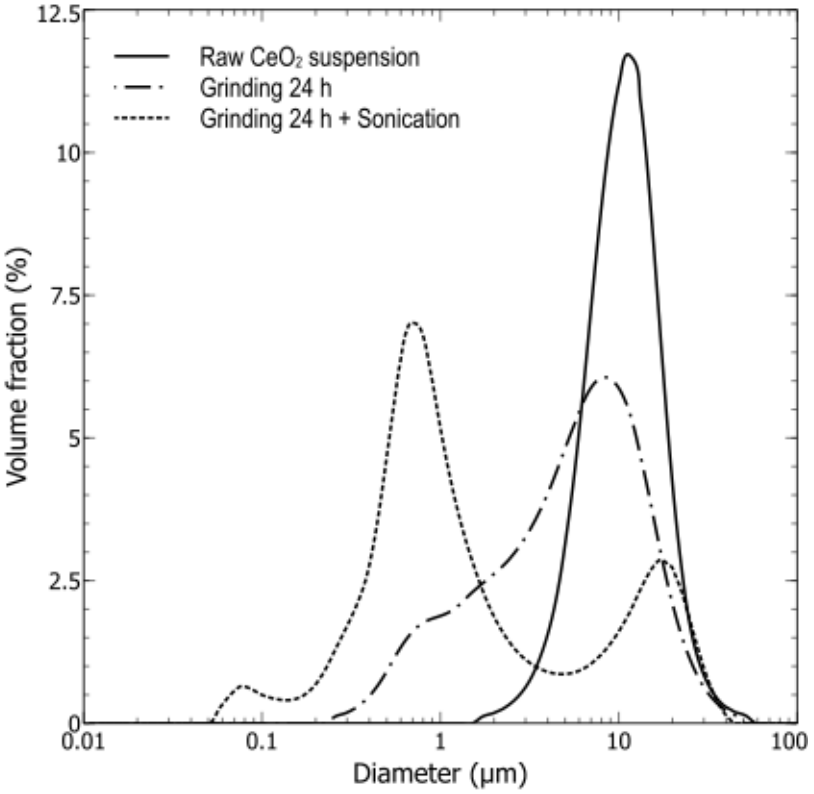

1-a

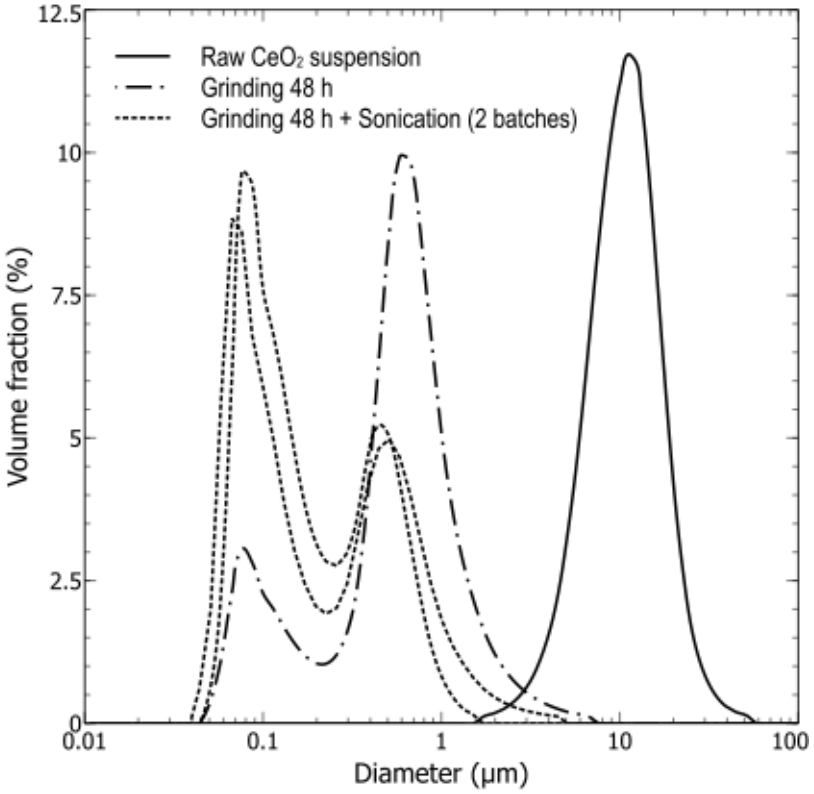

1-b

Figure 2

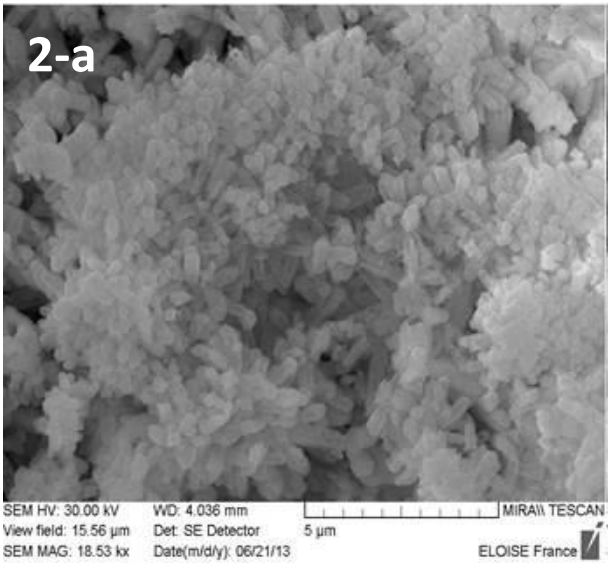
2-a
SEM HV: 30.00 kV
WD: 4.036 mm
MIRA\\ TESCAN
View field: 15.56 µm
Det: SE Detector
5 µm
SEM MAG: 18.53 kx
Date(m/d/y): 06/21/13
ELOISE France

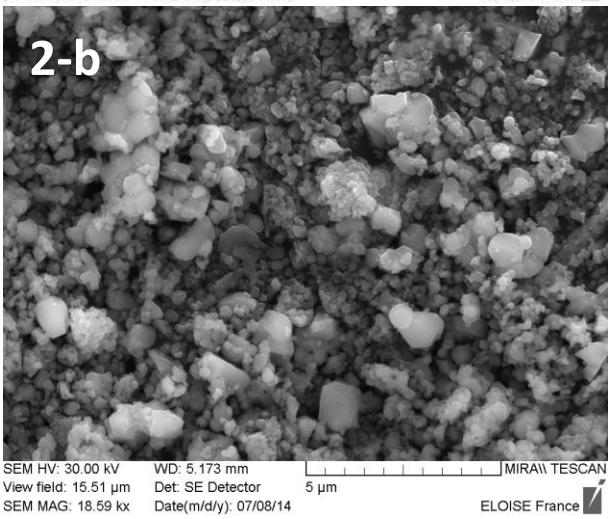
2-b
SEM HV: 30.00 kV
WD: 5.173 mm
MIRA\\ TESCAN
View field: 15.51 µm
Det: SE Detector
5 µm
SEM MAG: 18.59 kx
Date(m/d/y): 07/08/14
ELOISE France

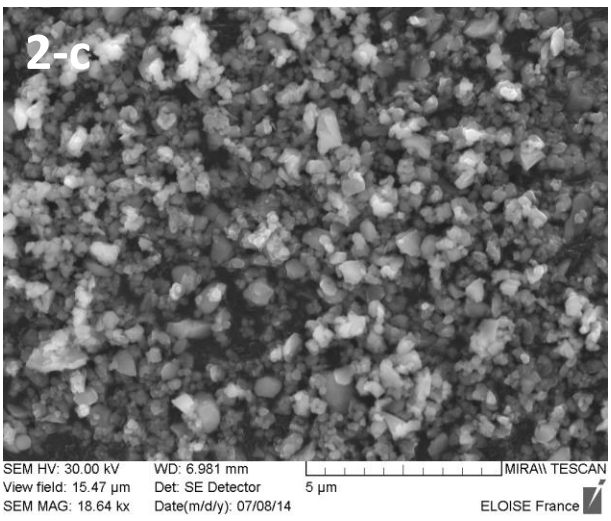
2-c
SEM HV: 30.00 kV
WD: 6.981 mm
MIRA\\ TESCAN
View field: 15.47 µm
Det: SE Detector
5 µm
SEM MAG: 18.64 kx
Date(m/d/y): 07/08/14
ELOISE France

Figure 3

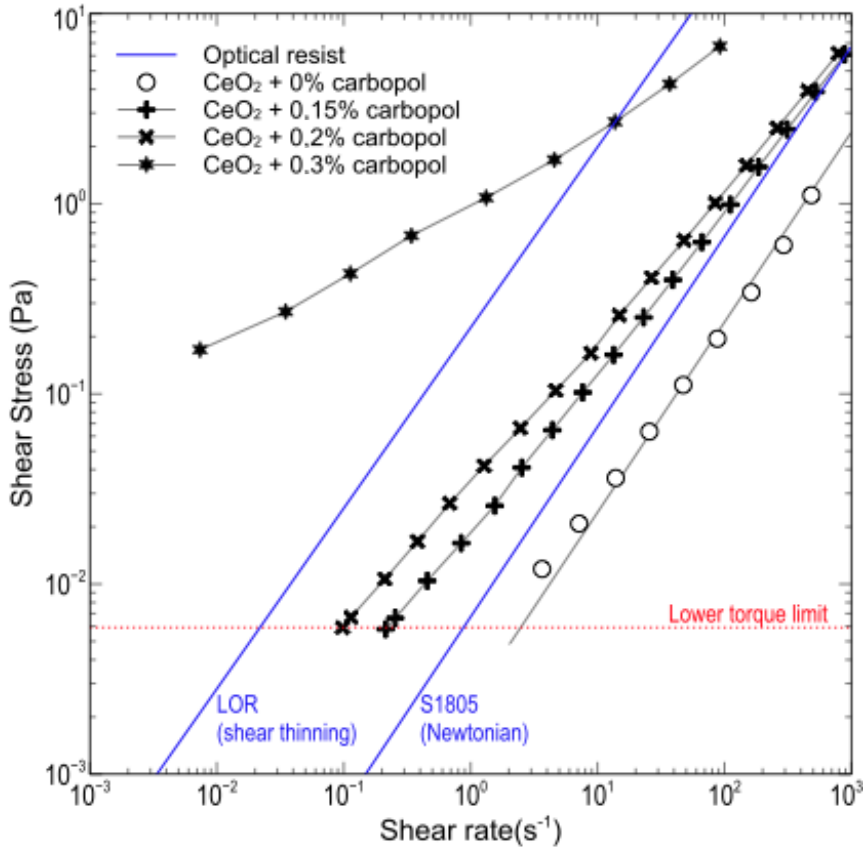
Optical resist
CeO2 + 0% carbopol
CeO2 + 0.15% carbopol
CeO2 + 0.2% carbopol
CeO2 + 0.3% carbopol
Lower torque limit
LOR
(shear thinning)
S1805
(Newtonian)
Shear Stress (Pa)
Shear rate(s-1)

Figure 4

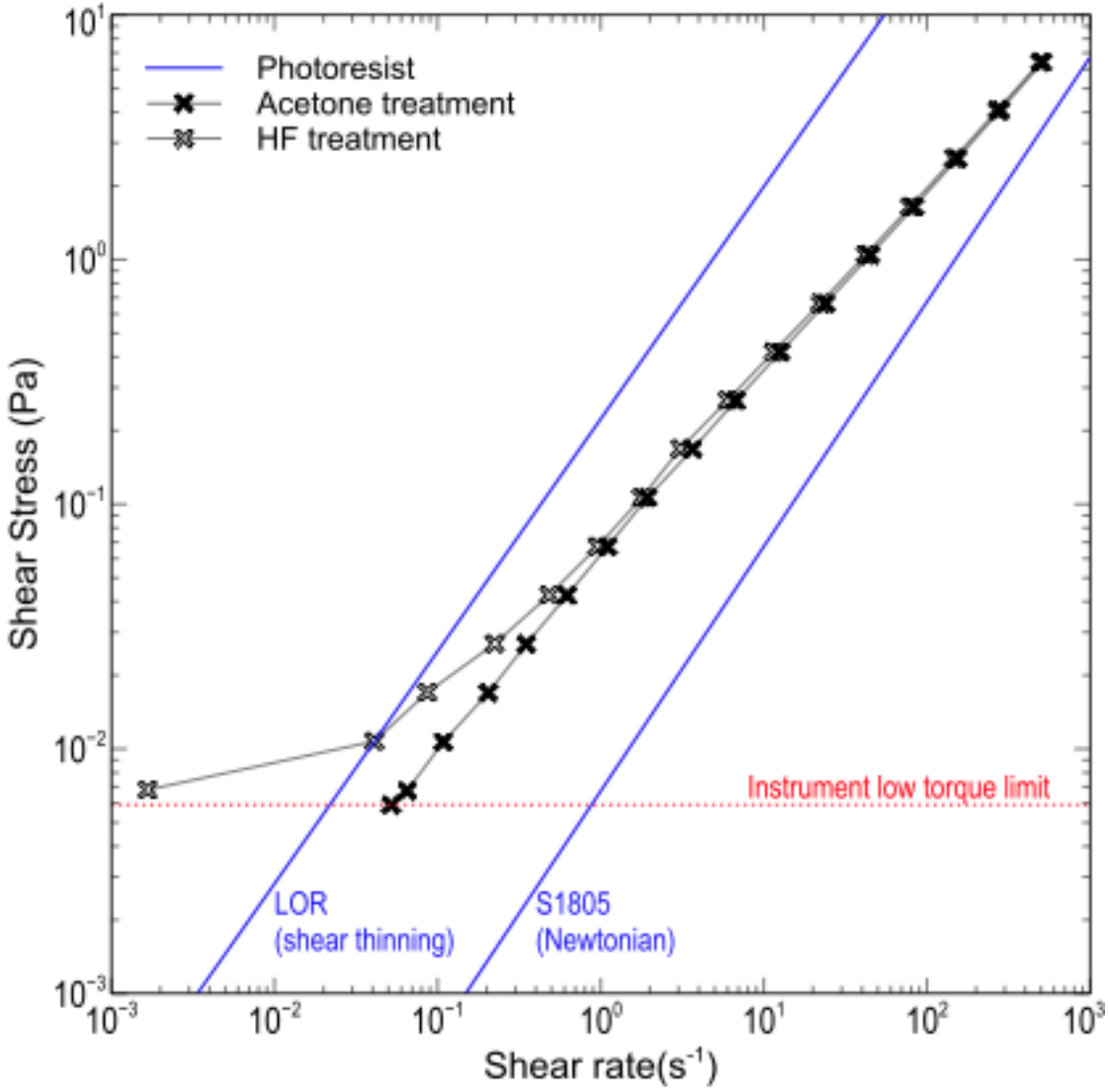
Photoresist
Acetone treatment
HF treatment
Instrument low torque limit
LOR
(shear thinning)
S1805
(Newtonian)
Shear Stress (Pa)
Shear rate(s^{-1})
10^{1}
10^{0}
10^{-1}
10^{-2}
10^{-3}
10^{-3}
10^{-2}
10^{-1}
10^{0}
10^{1}
10^{2}
10^{3}

Figure 5

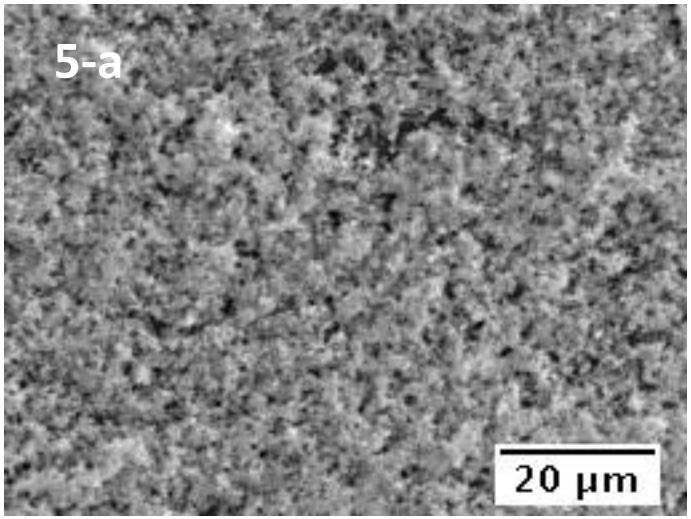

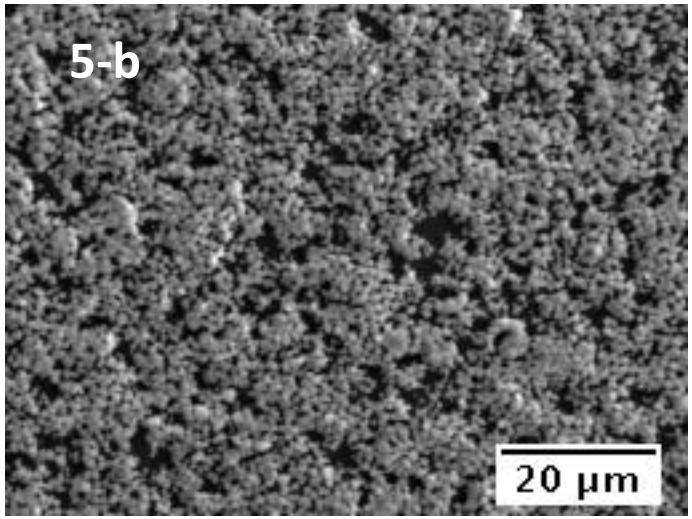

Figure 6

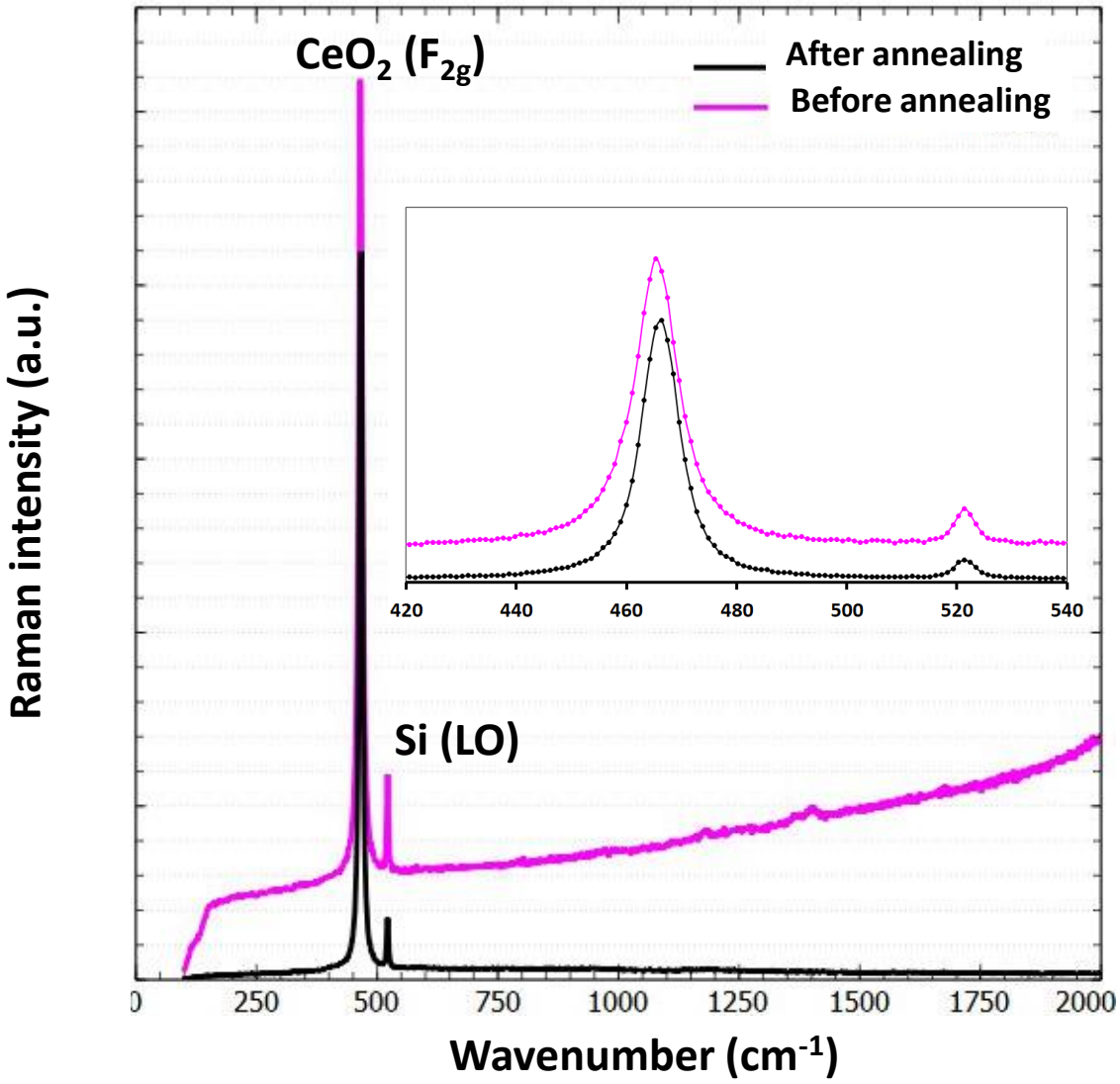
CeO2 (F2g)
After annealing
Before annealing
Si (LO)
Raman intensity (a.u.)
Wavenumber (cm-1)
0
250
500
750
1000
1250
1500
1750
2000
420
440
460
480
500
520
540

Figure 7

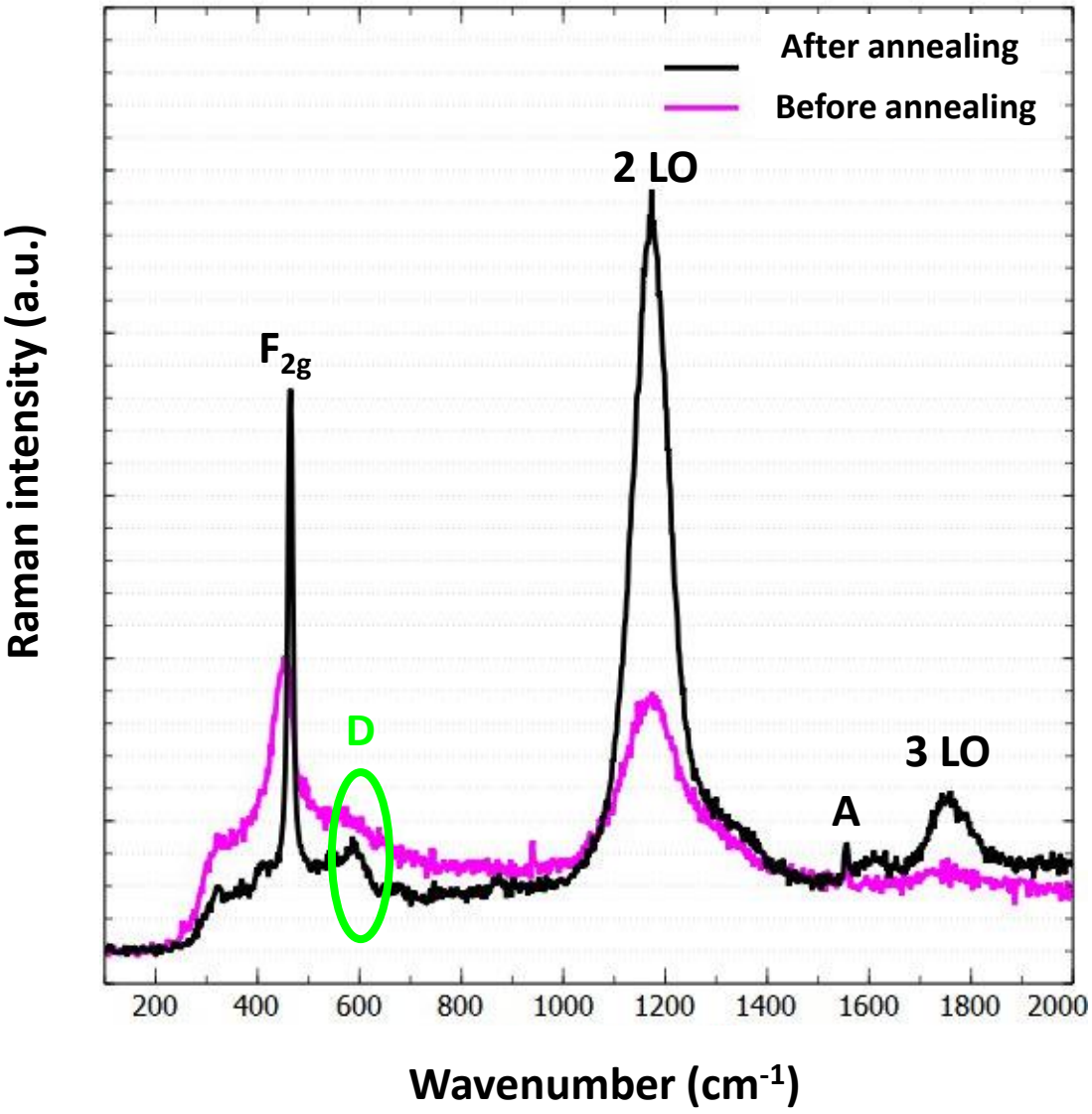
After annealing
Before annealing
2 LO
F2g
D
3 LO
A
Raman intensity (a.u.)
200
400
600
800
1000
1200
1400
1600
1800
2000
Wavenumber (cm-1)

Figure 8

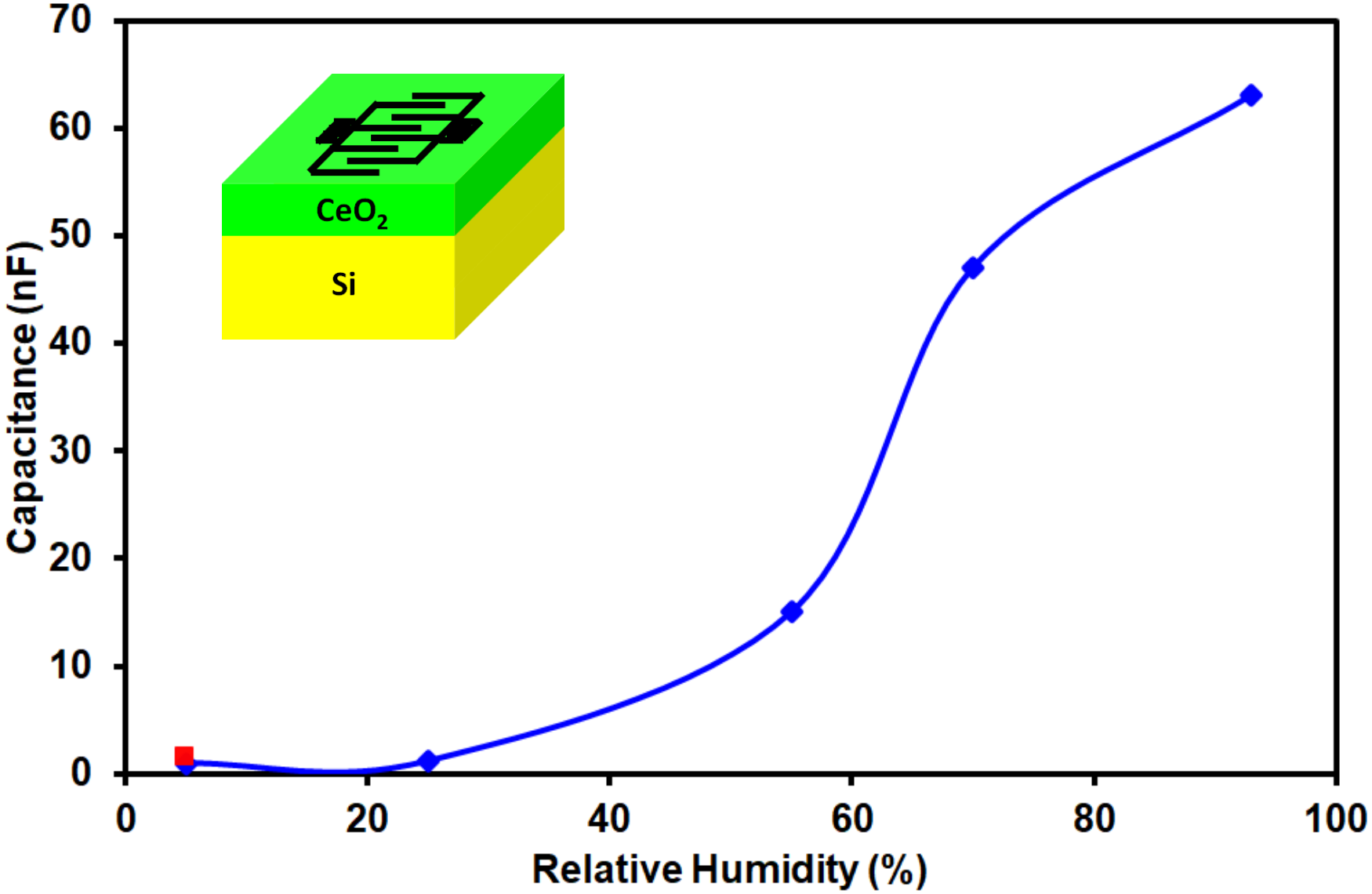
70
60
50
40
30
20
10
0
Capacitance (nF)
0
20
40
60
80
100
Relative Humidity (%)
CeO2
Si

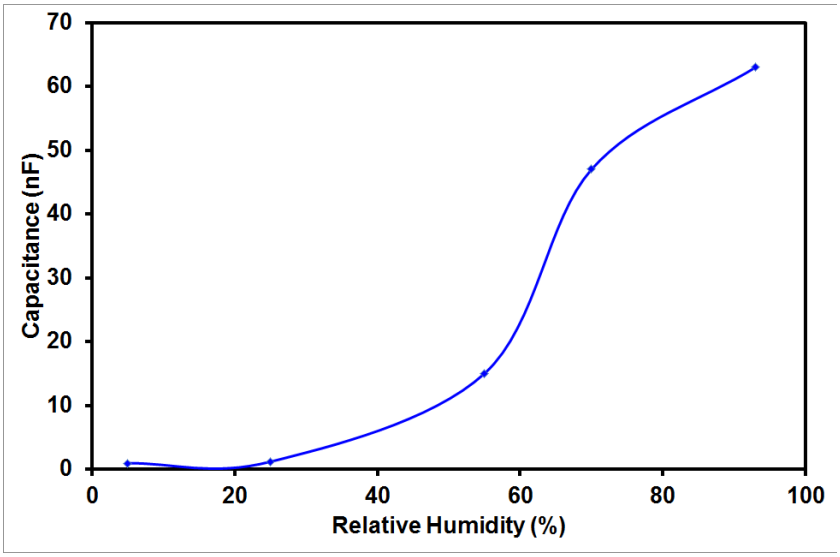

This figure presents the impact of the relative humidity on the capacitance of a sensor performed on a CeO_2 thick layer deposited on a silicon substrate by using a new process of deposition from a suspension of CeO_2 nanoparticles. First promising results on the humidity sensitivity have been shown.